# Land Cover Analysis of Kshipra River Basin Using LISS IV and CORONA Images: Comparison of Object Based and Pixel Based Classification

Ву



Centre for Ganga River Basin Management & Studies (cGanga)

# **Lead Persons**

- 1. Vinod Tare, IIT Kanpur
- 2. Shivansh Srivastava, IIT Kanpur

# 1. Introduction

Nature has blessed mankind with the sublime environment comprising of land, water, air, etc. These resources have served as substructures for human civilization. Man has used these natural resources to promote growth and turn prosperous. However, the increasing population rate and quadrupling developmental activities in recent years have resulted in an uncontrolled exploitation of these resources. The objective of an exalted human progress has been hit hard with ground implications of an excessive intervention in nature's earth. For instance, human settlements and agriculture are invading forest areas. Shrinking of rivers is also caused by human encroachments. Numerous polluting activities have also contributed significantly in bringing the planet to a miserable condition.

Land is one of the most important natural resources as it supports most of the development. Man has severely altered the land through his pace and magnitude of development. Land cover is the physical material present on the surface. It indicates, for example, how much of the land is covered by forest, water bodies, parks, etc. Land use is defined more anthropocentrically. It shows up the trend of human practices on any region such as developing or conservational activities. The distribution of land classes and its change with time due to natural or anthropogenic reasons has aroused the keen interest of researchers in generating land use and land cover (LULC) mapping.

Remote sensing is the science for capturing images of the ground and facilitates the modern LULC mapping. It has certainly helped in understanding the natural world to a great extent along with small degrees of humans and societies inhabiting the world. With recent developments, satellite systems of high resolution have emerged and provided a whole new platform for researchers to explore GIS and remote sensing technologies for human applications (Hay *et al.*, 1996). This study attempts to explore these tools and techniques for preparing land cover maps for reference and present conditions of Kshipra River Basin (KRB), a sub basin of the Ganga River Basin (GRB), for subsequent eco-hydrological studies of the basin.

# 2. Literature Survey

Kshipra is a small but culturally, spiritually and historically one of the important tributaries of the National River Ganga. The catchment area of the Kshipra River is approximately 5,700 km<sup>2</sup> in the south-west portion of the National River Ganga Basin (NRGB). The Kshipra river, originates on the Kokri Bardi hill (22° 31' N and 76° E, 20 km south-east of Indore near the small village of Ujeni), touches an industrial town Dewas and flows through Ujjain, a religiously important city. Ujjain hosts one of the four most

important events that occurs every twelve years (the other three places being Nashik, Haridwar and Allahabad). Millions of people visit Ujjain during this event (popularly referred as Simhasth) and take dip in the holy river. The Kshipra River (also referred as Avanti nadi) enters the city of Ujjain immediately after the confluence with Chandrabhaga (or Kanh) and flows in a northerly direction across the Malwa plateau to join the river Chambal.

As shown in Figure 1, river Kshipra flows in a general north-westerly direction and has a very sinuous course. The total traverse of about 190 km flows through Indore, Dewas and Gwalior districts of the state of Madhya Pradesh. The main tributaries of Kshipra include the Chandrabhaga (Kanh) river near Ujjain and the Ghambir river near Mahidpur.

Over the years the river has lost its perennial nature and now runs dry for a period of 5 to 6 months per year. Water of the Kshipra basin is used for drinking, industrial and irrigation purposes.

River Kshipra is facing serious problems of quantity and quality of water, and has essentially become drain carrying sewage and industrial effluents. In many stretches river space has been encroached for various activities detrimental to the health of the river. Dumping of solid wastes on river banks is a common site. As a result the river has become a backyard instead of serving as a lifeline. Citizens are concerned about such a dilapidated state of the river, particularly in the urban segments.

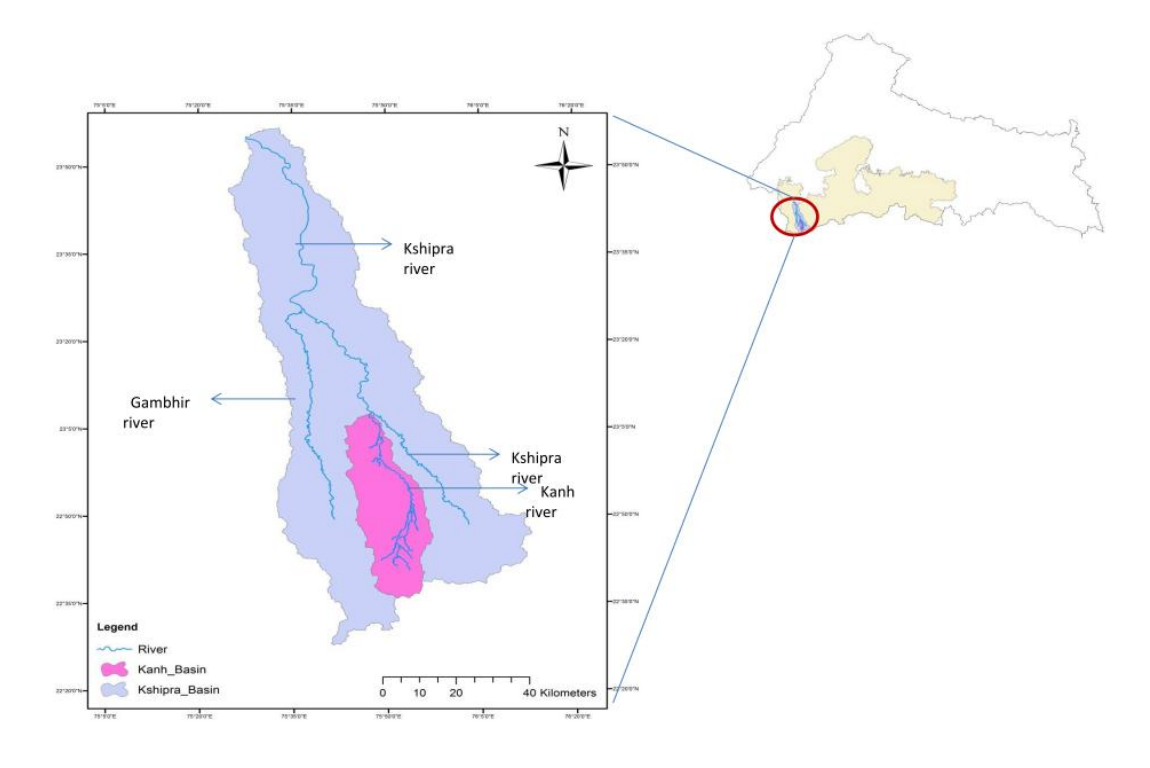


Figure 1: Kshipra River Basin Shown as Portion of Ganga River Basin

Hydro-ecological studies are very important to prepare river basin plans for rejuvenation of the rivers. The prerequisite to such studies is the analysis of land cover analysis. The most appropriate scientific approach for such analysis is the application of remote sensing techniques. As far as the KRB is considered, no substantial remote sensing studies have been reported. Land use and land cover patterns are not available for past and present situations. Despite vast remote sensing data coming from LANDSAT and modern high resolution satellites like QUICKBIRD, this portion of Madhya Pradesh has not been mapped. This certainly underlies the lack of historical land cover information. However, some studies related to monitoring and modeling of water quality has been carried out for this region.

A water quality study of the holy river Kshipra using Water Quality Index (WQI) was carried out to find the deteriorating condition of the river by Gupta *et al.* (2012). Parameters namely Temperature, pH, Turbidity, Total Solids, Dissolved Oxygen (DO), Biochemical Oxygen Demand (BOD), Phosphate, Ammonia and Fecal Coliform were determined at important locations of rivers Kanh and Kshipra for summer, monsoon and winter seasons in the year 2010. Assessment was made through Water Quality Index (WQI), a single number representing large quantities of data. The results showed that the water in Kshipra is not even up to bathing standards. The study also indicated that river Kanh is the major tributary polluting Kshipra.

In another study, Gupta *et al.* (2014) examined the water quality of Kshipra basin with an objective to suggest measures for bringing the river waters to bathing standards. A stream water quality model, QUAL-2K was also used to simulate the contributions from different sources and sinks of dissolved oxygen, and to understand the interactions among them.

A GIS based study had also been conducted in order to identify the soil erosion susceptible regions (Omar, 2015). It recommended a conservation plan for sustainable development of Kshipra catchment area. SRTM data were used to analyse the morphology of the basin in order to attain drainage characteristics. This work also emphasized on the capabilities of remote sensing and GIS techniques in preparation of holistic watershed management plans.

Available literature indicates that no comprehensive studies related to land use and land cover changes are available for the Kshipra basin. This work was taken up to produce a reliable comparison of land cover in the mid-1960s and 2013 for the KRB. It was found through review of literature that object based techniques are replaceing the pixel based techniques to a great extent in modern LULC studies (Blaschke, 2003). Thus for the land use and land cover mappings of the KRB, object based approach may be adopted.

Conventionally, studies and analyses of remote sensing data were based on pixel-based methods. Per-pixel analysis of the satellite imageries using supervised and unsupervised algorithms were limited to the spectral information sustained by pixels. Toll (1984) and Martin *et al.* (1988) carried out a study to compare the extraction results of pixel based technique using Landsat MSS (Multi-spectral scanner), TM (Thematic mapper) and SPOT imageries of the same area. They observed that nominal statistical analysis technique will not drive the classification process at higher accuracy. These methods limit the potential for a detailed and reliable mapping due to their resulting in the salt and pepper classification (Stumpf *et al.*, 2011).

Achieving a desirable accuracy became further unattainable with the emergence of high satellite imageries. Researchers gradually started targeting the shortcomings in the traditional approaches. Blaschke and Strobl (2001) have thrown light on the reluctance of remote sensing groups on using the patterns formed by group of pixels. They advocated this viewpoint on having identified an increasing dissatisfaction with pixel-by-pixel image analysis. Similarly, Cracknell (1998) and Burnett and Blaschke (2003) observed something which was beyond pixels. The flight of these questions and understanding on remote sensing arrived on a platform known as object based image analysis (OBIA) (Burnett and Blaschke, 2003; Liu *et al.*, 2006; Blaschke*et al.*, 2003; Lang and Blaschke, 2006).

Like modern remote sensing satellite data, historic data from CORONA satellite have also not been used to perform land cover analysis of KRB during 1960s though the historical data has come into use extensively worldwide. Many studies show that attaining the land cover patterns in the past and observing the changes in the present scenario have become inevitable for planning, constructional and developmental activities.

Kressler *et al.* (2003) studied the land use and land cover change in the city of Vienna using panchromatic images from KOMPSAT-1 and SPOT-5 data. The study concluded that using the fine spatial information in conjunction with the shape, size and neighborhood properties is helpful in obtaining the land cover changes in panchromatic images.

Ratcliffe and Henebry (2003) conducted a study to recognize the urban land cover change in Kazakhstan through historical pan-chromatic images. CORONA and GAMBIT images were used against the contemporary digital images of Quickbird satellite system. Observed types of urban change included expansion, landscape transformation and afforestation. Roads and buildings were also distinguishable.

Observed results show that there is more densification of urban areas in 2002 as compared to small patches in 1964.

In another land use and land class assessment study done on the drylands of Sudan, CORONA images were used to project the situation of past. To compare the area with present, IKONOS imageries were used. The study demonstrated the change that has occurred between 1969 and 2002. The results show that there is a 7% hike in cropland region as compared to 1969. The cropland was more scattered in 2002, while it was concentrated to the southern part of the study area in 1969.

Similar kinds of studies have been carried out by researchers worldwide to obtain LULC mappings. These studies focused on observing the changes in forest ecosystems, water bodies and built up areas (Dittirich *et al.*, 2010, Song *et al.*, 2010).

# 3. Objectives

To study the ecology, hydrology and geomorphology of any catchment area, land use and land cover (LULC) mappings play a significant role. These LULC patterns are utilized in resource management and planning activities (Kushwaha *et al.*, 1996). Till date, there is no significant remote sensing information related to land use and land cover patterns available for the Kshipra River Basin (KRB). The primary objective of this study is to establish LULC changes that have occurred in the KRB from the mid-1960s to 2013.

This work is also motivated by the proven superiority of object based image analysis (OBIA) over traditional pixel based classification approaches. OBIA methods overcome the drawbacks in pixel based methods and perform image classification with enhanced accuracy. The comparison between the two approaches is manifested by comparing the classification mapping produced by pixel and object based techniques.

Specifically, the research work has been carried out on following lines.

- 1. Selecting the satellite images for reference (1960-65) conditions (declassified US Spy Satellite CORONA images) and present (2013-15) conditions (LISS IV images).
- 2. Performing image classification using Object Based and Pixel Based analysis.
- 3. Comparing results of Object Based and Pixel Based analysis and producing Land Cover maps for reference conditions and present conditions.
- 4. Analysing Land Cover changes between reference and present conditions.

# 4. Study Area

This study is carried out on Kshipra River Basin (KRB), a sub-basin of the Ganga River Basin (GRB). It is located at the south-western periphery of the GRB (refer Figure 1). The Kshipra is a river in Madhya Pradesh state of central India, also recognized by the name Avanti. The total course of the river is around 195 km, flowing in the districts of Indore, Dewas and Ujjain. River Kshipra is a tributary of Chambal which in turn is a tributary of River Yamuna (ADB Report, 2011). Figure 2 shows KRB as part of the state of Madhya Pradesh covering districts of Ujjain, Indore and Dewas.

Kshipra originates from the Kokri Bardi hills (about 750 m above MSL, 22° 31' N and 76° E) in Vindhyanchal Range and flows in northern direction across the Malwa Plateau to join the Chambal River. Before its confluence with Chambal, Kshipra drains approximately an area of 5700 km². The basin lies between latitudes 22° - 24° and longitudes 75° - 76°. The river is well known for its sacredness and religious importance (ADB Report, 2011). It is considered as holy as river Ganga. The city of temples, Ujjain, is situated on the right bank of Kshipra. Thousands of Hindu shrines are situated along sacred river ghats of the river. The 'Simhastha Mela', a massive religious gathering in which millions of devotees take holy dip in the river, is organized every 12 years in the city of Ujjain, the next one being in April-May 2016.

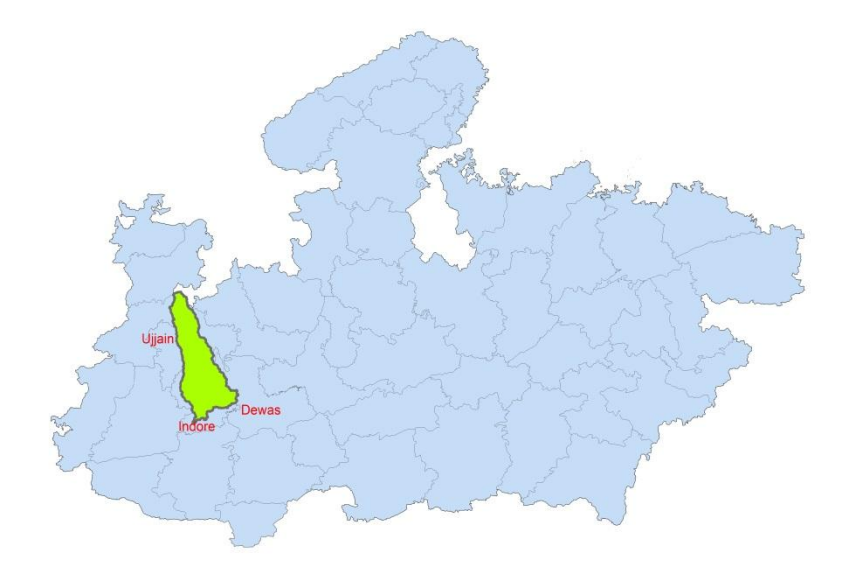


Figure 2: Kshipra River Basin as Part of the State of Madhya Pradesh

Over the years the river has lost its perennial nature and now remains dry for a period of 5-6 months in a year. The water from the river is mostly used for agricultural purpose. There are several villages situated along both the banks which drive out the water for irrigation purpose. It has two major tributaries contributing to its catchment:

Chandrabhaga (also known as Kanh) and Gambhir. Both these tributaries are seasonal and contribute majorly during the monsoon period only. River Kanh flows through the heart of the city of Indore and joins Kshipra upstream of Ujjain. River Gambhir flows from south to north piercing Mhow tehsil in Indore district and confluences with Kshipra near Mahidpur (ADB Report, 2011).

# 5. Pixel and Object Based Approaches

The motivation behind the satellite imageries lies in identification of similar objects that exist in the real world and in the images. Since remote sensing emerged, it has been overcoming its limitations with continuous development in its spectral information. However, the usage of only spectral information conceived by images is not enough. In order to achieve an accurate and realistic mapping, groups of pixels that comply with similar type of land cover objects have to be delineated and then classified in certain pre-defined classes.

## 5.1 Pixel Based Approach

Pixel refers to the smallest unit in the satellite images from which land cover information is derived. The spectral values associated with the pixels are used to allocate them to a land cover class to which they belong (Lillesand, 2001). The classification process is performed on per-pixel basis where it can be allocated to a single class only. There are two types of traditional pixel based classification methods: supervised and unsupervised classification.

The unsupervised classification method does not involve the user explicitly. The user just needs to specify the number of spectral classes that are intended. The algorithm segregates the image data into desired number of classes automatically. Later on the user can merge or split the various classes to obtain a realistic land cover mapping. The unsupervised method is preferably used when there is uncertain information on the land cover distribution. There are numerous classification algorithms that can be used to group the image pixels into spectral classes in a data set. The most commonly used method for clustering is known as K-means algorithm (Agarwal and Procopiuc, 1998).

The supervised classification method proceeds with the aid of an analyst in the form of representative samples for each land cover class desired. Training samples are selected all over the image which resemble the spectral values permitted in a land cover class. After selecting the training samples, a classifier is chosen to obtain the classification. Some of the classical classifiers are maximum likelihood classifier, parallelepiped classifier and minimum distance to mean classifier (Jain, 1986). Pixels with unknown identity are then compared numerically with the spectral values of training samples

and labeled to a land cover class according to their cognizance and similar spectral characteristics with training samples.

## 5.2 Object Based Approach

The reason behind the shifting of remote sensing fraternity to object based analysis is its ability to combine the multiple random pixels into meaningful homogenous areas (Blaschke, 2003). With advanced satellite systems producing imageries of very fine resolution, object based approaches have become inevitable for land cover mappings. The vast spectral variability in high resolution images and the ability of OBIA to generate meaningful objects has outperformed the traditional approaches.

The classical pixel based techniques for classification does not have any regard for spatial and textural information in the image. To overcome this drawback, object based image analysis was introduced. The fundamental process involved in OBIA techniques is known as image segmentation. Image segmentation can be defined as dividing the image into non-overlapping and continuous objects, also referred as segments. Segments are homogenous areas in the image space which have similar properties of one kind and very different properties of some other kind. Numerous techniques like Threshold based, Region based and Edge based segmentation are available in order to attain desired segmentation results (Rohan *et al.*, 2014). Next to segmentation is matching of real world objects with the segments produced. The image objects should be accurately matched to produce realistic land cover patterns.

Working with segments is a lot easier and more accurate in comparison with that of pixels. Computational load is highly reduced as object based methods combine pixels into a group which is homogenous in one or more sense, thereby averting the interpretation of individual pixels. It has found vast applications in the field of medical imaging, object detection, traffic control systems, video surveillance, recognition tasks, etc. However, the focus in this study will be predominantly on object detection.

## 6. Datasets

# 6.1 LISS IV Images

7 satellite images were procured from National Remote Sensing Center (NRSC). These images were acquired from the RESOURCESAT-2 satellite system capturing images with ground resolution of 5 meters. Following are the details of the satellite images obtained (Table 1):

Table 1 : Details of LISS IV Satellite Imageries Used in the Study

S No	Path	Row	Acquisition Date
1	95	55B	15 Dec, 2013
2	95	55C	26 Nov, 2013
3	95	55D	15 Dec, 2013
4	96	56A	26 Nov, 2013
5	96	56B	20 Dec, 2013
6	96	56C	26 Nov, 2013
7	96	56D	20 Dec, 2013

## 6.2 CORONA Images

Originally, the CORONA images were marketed in the form of film negatives or photo prints. Since 2004 these images are provided to users in digital formats (Galiatsatos, 2009). For this study, 11 CORONA frames were procured in the Tiff (.tif) format. Each of the corona frames is provided with 4 overlapping segments. All the images had scanning resolution of 7 microns. The other information related to the imageries is presented in Table 2.

Usually there are limited sets of images available for any area that got photographed during the CORONA mission. The user needs to identify the best of all, as the clarity in the images may be obscured by clouds. While selecting, cloud free images were chosen on priority. The set of procured images covered an area much larger than that of the Kshipra River Basin.

Table 2: Details of CORONA Satellite Imageries Used in the Study

S	Entity ID	Centre C	oordinates	Camera	Acquisition Data	
No	Entity-ID	Latitude	Longitude	Resolution	Acquisition Date	
1	DS1021- 1055DA039	24.11	75.992	Stereo Medium	22 May 1965	
2	DS1021- 1055DA040	23.96	76.029	Stereo Medium	22 May 1965	
3	DS1021- 1055DA041	23.81	76.071	Stereo Medium	22 May 1965	
4	DS1021- 1055DA042	23.66	76.104	Stereo Medium	22 May 1965	
5	DS1021- 1055DA043	23.5	76.146	Stereo Medium	22 May 1965	

6	DS1021- 1055DA044	23.35	76.184	Stereo Medium	22 May 1965
7	DS1021- 1055DA045	23.2	76.221	Stereo Medium	22 May 1965
8	DS1021- 1055DA046	23.05	76.263	Stereo Medium	22 May 1965
9	DS1021- 1055DA047	22.89	76.296	Stereo Medium	22 May 1965
10	DS1021- 1055DA048	22.74	76.342	Stereo Medium	22 May 1965
11	DS1021- 1055DA049	22.59	76.375	Stereo Medium	22 May 1965

CORONA images suffer from geometric distortion, maximum at edges. Hence, while browsing and ordering images, their orientation with respect to the study area was kept on watch. The study area lay in the centers of the frames, thereby experiencing minimum distortions. This reduces the efforts that need to be put in while georeferencing the images.

# 7. Methodology

# 7.1 LISS IV Images

To satisfy the objectives of this work, certain land use and land cover classes were selected and mapped on the satellite images. Table 3 lists the land covers that were used along with their physical inclusions on ground.

Table 3: Land Use and Land Cover Classes to be identified from the Satellite Images

SNo	Major Class	Inclusions
1	Water	Rivers, Ponds, Drains, Marshlands
2	Urban	Buildings, Roads
3	Agriculture	Land with and without crops where agriculture is practiced at
		least for some part of the year, Grasslands
4	Barren	Land where agriculture is not practiced, Sand bars, Rocky lands
5	Tree Cover	Trees, Thick shrubs

### **1.1.1** Pixel Based Classification

In total seven frames from LISS IV sensors were procured from the National Remote Sensing Centre, India (NRSC). The spatial resolution of the images is nearly 5.8 m with

each image having three spectral bands. These bands can be identified as Green, Blue and Near Infra-red band. All the processing work was carried out on ARCGIS platform.

First, individually the bands in each of the seven images were sacked to obtain a composite band image. These composite band images were mosaicked to form a single image showcasing an overall area. However, the study was focused only on Kshipra basin, so the area of interest was extracted using mask tool.

The next task was to identify the spectral responses that should be collated to obtain a reasonable mapping of the study area. After finalizing the classes, it was needed to detect them in the image data set. Training samples were chosen across the image in order to cover the spectral ranges for the selected classes. This was ensured by selecting numerous samples for each class. Also, the training samples were chosen such that they resemble the digital numbers of their corresponding classes. It was done to safeguard and eliminate the inappropriate values that might deceive the spectral range formed by the training samples. Therefore the training sites were selected at those image spaces where edges of two different classes do not overlap with the common sample. To carry the process further, maximum likelihood classifier was used to perform the supervised classification. On successful classification, accuracy assessment was performed to judge the dwelling errors in this traditional approach.

Often there is ambiguity on the accuracy assessment strategies in which random points are chosen across the image. There is always room for reflecting higher accuracy while selecting the random check points and identifying if the classified pixel belongs to its corresponding land cover. In other words, classification accuracy can be altered by choosing the correctly classified points and excluding misclassified points in the array of random points prepared for assessing the accuracy. However, such misinterpretations and delusions should not occur in any research work, unintentionally though.

The authenticity of this study was maintained by applying a handy assessment strategy. The entire basin area was divided by grids. The check points are selected in each of the grids such that there is minimum inclusion of human factors that might lead to erroneous accuracy assessment. Nearly 100 points were chosen in each of the classified spectral responses and were checked against their actual land cover class using Google earth imageries.

It was seemingly plausible to detect the erroneous classification occurring in the process by witnessing the classified image. On inspection it was found that the urban class invaded into the river course. Sand bars lying at regular intervals along the river

got merged with the urban class. Next, some of the barren land is also confused with agricultural land. A nominal misclassification was also observed between moist agricultural land and water class.

All these classification errors can be attributed to similar spectral information carried by some of the pixels in different classes. Such errors cannot be checked unless there is a manual assignment of misclassified regions to their respective correct classes. However, it breaches the objectives of a meaningful classification. Eventually, to improve the classification, an object based analysis was carried out on the same image.

#### **1.1.2** Object Based Classification

Object based image analysis was performed on the extracted image of the basin used in per-pixel based method. The following paragraphs cover the methodology used for the classification.

#### a) Segmentation

The heart of any object based analysis lies in meaningful segments generated from combining the pixels. In this study, a multi resolution segmentation process was performed using the software tool eCognition 9.1 at various scale parameters such as 5, 10, 15, etc. The shape and compactness criteria were also adjusted at various values in order to achieve a successful segmentation. The default value for shape and compactness are 0.1 and 0.5 respectively. Layer weightages were kept as default which is equal to 1 for all layers. The segments were made as fine as possible in order to reflect their original classes without any ambiguity by exploring the segmentation parameters vigorously.

#### b) Rule set generation

Rule sets are the series of algorithms that are prepared to classify satellite imageries. For this study, separate rule sets were developed to extract the classes of interest. Rule sets were prepared thoroughly using various object features available with the software suite. It involved using textural properties of the surfaces along with the spatial and spectral information available. For instance, to highlight the urban class the object feature GLDV contrast in conjunction with a customized arithmetic feature derived from the spectrally available information was used.

Similarly, rule sets were developed for each class to attain a favorable extraction of objects and distinct classification.

#### c) Extraction and accuracy assessment

The classified segments were then exported to ARCGIS 10.0, which finally showed up the entire classified basin. Accuracy assessment was performed using

the same check points that were developed while performing pixel based classification.

## 7.2 CORONA Images

#### 7.2.1 Pre-processing

The size of a CORONA film is much larger than the photogrammetric scanner used to produce digital formats. Therefore, overlapping subsets of entire images are supplied by the USGS. Stitching these subsets is necessary before performing any operation on the CORONA images. Various image stitching and processing software's are currently available. Adobe Photoshop was found to be the most suitable among the existing methods (Sarkar, 2014).

The images shown in Figures 3 to 6 are subsets of a bigger area which can be perceived on combining them. On close inspection one can observe that there are overlapping regions in each of the images.

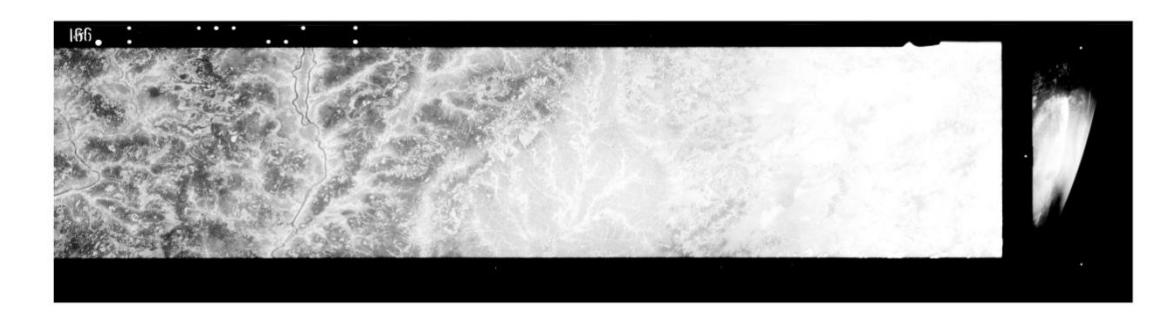


Figure 3: Corona Image DS1021-1055DA042\_a



Figure 4: Corona Image DS1021-1055DA042\_b



Figure 5: Corona Image DS1021-1055DA042\_c

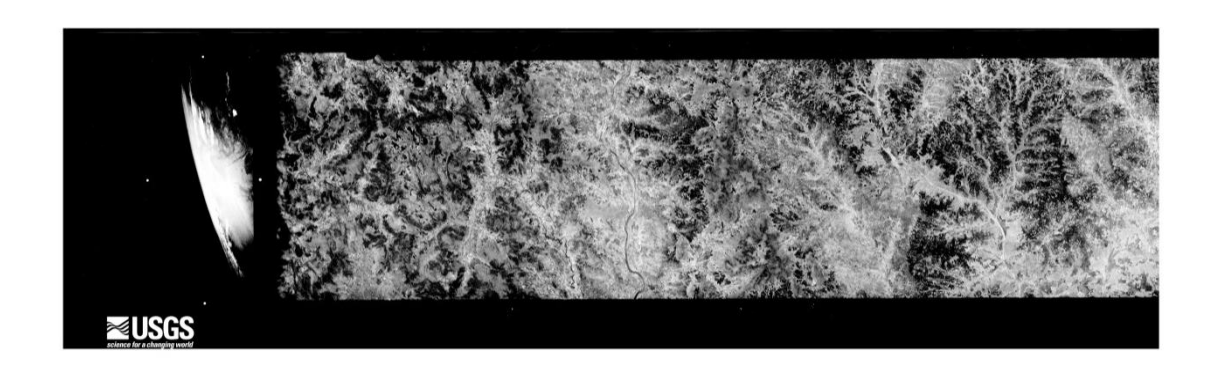


Figure 6: Corona Image DS1021-1055DA042 d

For this work the Photomerge tool available in Photoshop was used to stitch the individual segments into one single complete image. There are several layout options available in Photomerge such as cylindrical, spherical, collage, etc. But, Reposition mode was used in the operation as it does not transform the image. Reposition aligns the layer and matches overlapping segments without stretching the image. Photoshop then merges all the segments and provides a single overall picture.

The next task is to reduce the different layers into one single background layer. Flattening option flattens all the layers and reduces the file size considerably. After flattening, the image is transformed into a grayscale image. A workflow diagram for pre-processing the CORONA images and using them for further operations is shown in Figure 7.

Finally, the cropping of the extraneous and undesirable black edges is done to make the image ready for further operations. This again reduces the size of an image. A preprocessed image shown in Figure 8 is then used for ortho-rectification and subsequently forming the complete study area.

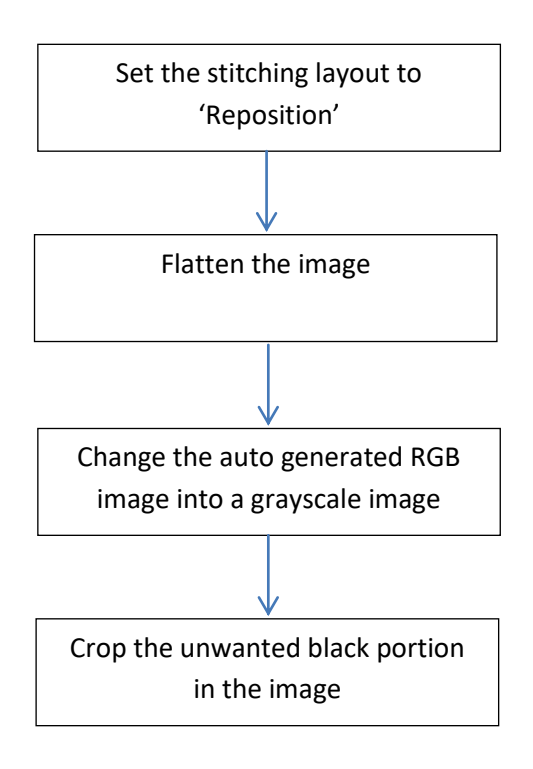


Figure 7: Workflow of the Pre-Processing Process



Figure 8: Overall Region by DS1021-1055DA-042

#### 7.1.2 Ortho-rectification

After the pre-processing operations, the CORONA images are ready to be georeferenced. The orientation and spatial information are incorporated in the images by using the Ground Control Points (GCPs). To put up any spatial information, coordinates of GCPs are matched to the corresponding points in unreferenced images. There is requirement of a base map i.e. an image which is spatially accurate or a set of points collected through ground surveying. Though detecting the points by investigation on ground is an option, it is intensively laborious and time consuming. So, the best choice is using base maps and identifying the points which could be successfully matched in non-referenced images.

Base maps are available online. Some examples of these are Google maps, Bing maps and Open Street maps, etc. The distinct features or objects are identified in the base maps and their location is matched in the unreferenced images. Bing maps use a projected coordinate system called Mercator Auxiliary Sphere, which uses GCS\_WGS\_1984 as its geographic coordinate system. The datum used in the Bing maps and Google earth is WGS 1984. If the geographic coordinate system of the source data

does not use the WGS 1984 datum then it is required to apply a transformation to the data in order to align correctly with Google Maps and Bing Maps (Galiatsatos, 2004).

For this study, Bing maps were used for the georeferencing. The projected and geographic coordinate systems along with the datum were closely inspected before georeferencing the CORONA images against them. Since the area of interest lay in middle of the frames, relatively more GCPs were chosen at the centers of the images. This further helped in standing against the geometric distortion suffered at the corners. More than 100 GCPs were chosen in order to assign the coordinates that were distinct and identifiable in both the unreferenced images and the base map.

After a superficial observation on the orientation of the frames with respect to the base map, second order polynomial function was used to stretch the frames. Stretching of the image tackles the complex geometric distortion. The polynomial transformation uses a polynomial built on control points and a least-squares fitting algorithm. The polynomial transformation yields two formulas: one for computing the output x-coordinate for an input (x,y) location and one for computing the y-coordinate for an input (x,y) location. The goal of the least-squares fitting algorithm is to derive a general formula that can be applied to all points, usually at the expense of slight movement of the positions of the control points (ArcGIS 10 Help document). Figures 9 to 12 show the images after applying different transformations.



**Figure 9: First Order Polynomial Stretching** 



Figure 10: Second Order Polynomial Stretching



Figure 11: Third Order Polynomial Stretching



Figure 12: Spline Stretching

Next, the individual frames were mosaicked using ArcMap10 as shown in Figure 13. This resulted in an overall picture of the area for which the CORONA images were ordered. Kshipra basin was extracted from the mosaicked image using shape file for the basin as a mask. The size of image that will be used for further operations is thus reduced, which in turn increases the computational speed.

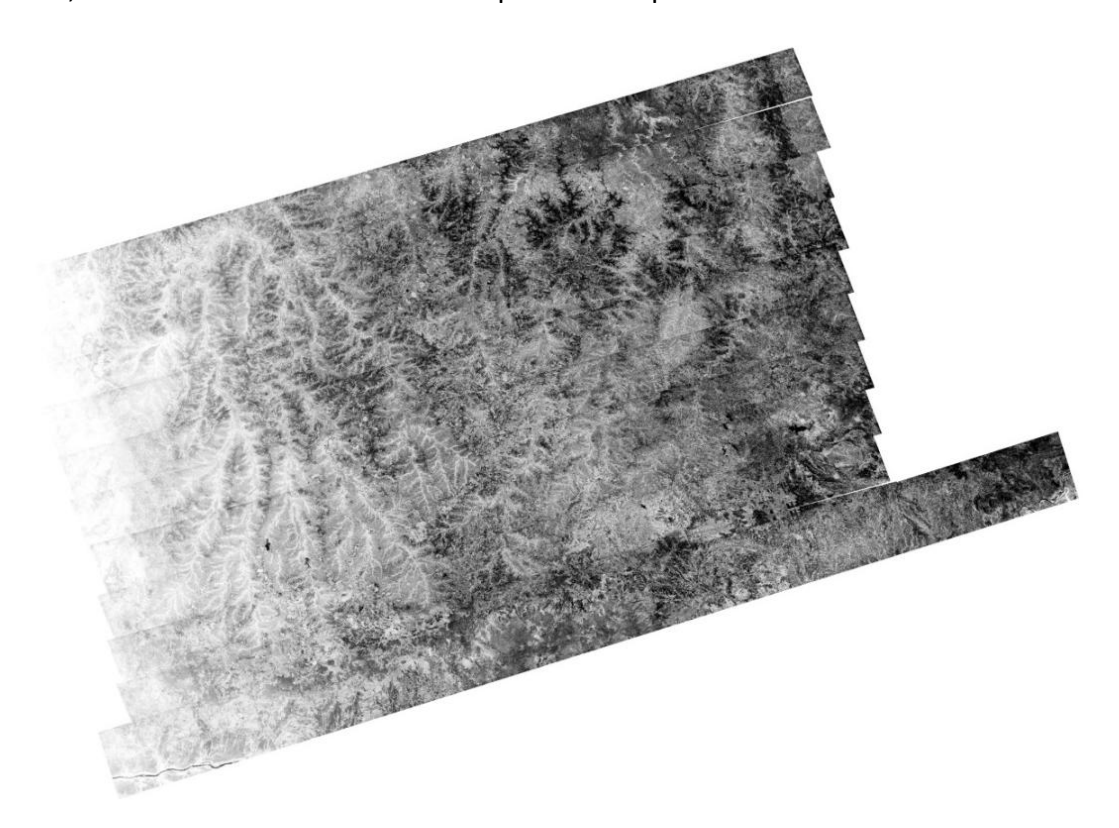


Figure 13: Mosaic Image Obtained by Combining all the Frames

#### 7.1.3 Classification

Since the CORONA images do not possess significant spectral information, pixel based classification techniques are unsuccessful in classifying them. The pixel values for different land cover classes are similar which limits the application of traditional pixel based technique on panchromatic images.

For this study, spectral information from the CORONA images is combined with the textural and contextual information. Firstly, a segmented image is obtained by applying the multi-resolution segmentation algorithm on the image. Secondly, the objects formed were closely scrutinized on the basis of their pixel values. Thirdly, the spectral values are used to highlight the land cover features and then they were assigned to their respective classes according to their texture and context properties.

For instance, pixel values for trees are similar to some portions of agricultural lands. They both were separated using the shape and neighborhood properties of the objects

falling under the two land cover classes. Trees generally have smaller area in comparison to the Agricultural fields. Also, the shape for agricultural fields is mostly rectangular. A threshold value is determined for these object features and classification is performed. However, there were marginal misclassifications, which are needed to be rectified manually.

# 8. Results and Discussions

## 8.1 Object Versus Pixel Based Classification

The LISS IV images were classified using traditional pixel based and emerging object based classification methods. Object based classification showcases the edge it has over per-pixel classification. The accuracy assessment done with 500 random points clearly depicts the enhanced accuracy obtained by object based classification technique. Google earth images are used as reference source for assessing the accuracy of classification.

Total or Overall accuracy can be calculated as the ratio of correctly classified points to the total number of points. Tables 4 and 5 demonstrate the error matrices used to calculate the overall accuracy of the two classification methods. In the tables, the diagonal elements reflect the correctly classified points. Using the concept:

$$Overall\ Accuracy = \frac{Number\ of\ correctly\ classified\ points\ for\ a\ class}{Total\ number\ of\ points\ for\ a\ class}$$

Pixel based classification provided an overall accuracy of 84.2% in comparison to the object based classification with 94.6% accuracy.

However, computing the overall accuracy represents the average classification accuracy. It is devoid of showcasing the error occurring in the individual classes. In other words, it does not reveal whether the error is distributed evenly or concentrated to specific classes. Therefore, producer's and user's accuracy are also determined. User's accuracy corresponds to the error of commission or inclusion. Producer's accuracy corresponds to the error of omission or exclusion.

User's accuracy is calculated for each class as:

User's Accuracy

 $= \frac{\textit{Number of correctly classified points in classified map for a class}}{\textit{Total number of points in classified map for a class}}$ 

Producer's accuracy is calculated for each class as:

## Producer's Accuracy

 $= \frac{Number\ of\ correctly\ classified\ points\ in\ reference\ source\ for\ a\ class}{Total\ number\ of\ points\ in\ reference\ source\ for\ a\ class}$ 

**Table 4: Error Matrix for Object Based Classification** 

#### Referenced

Classes Water **Agriculture** Urban **Barren Forest** Total Water **Agriculture** Urban **Barren Forest** Total 

**Table 5: Error Matrix for Pixel Based Classification** 

#### Referenced

**Classes** Water **Agriculture Forest** Urban **Barren** Total Water Agriculture Urban **Barren Forest** Total 

The user's and producer's accuracy for each class in both classification methods is shown in Table 6.

Table 6: User's and Producer's Accuracy for Pixel and Object Based Methods

Classes	User Accuracy (%)		Producer A	ccuracy (%)
	Pixel	Object	Pixel	Object
Water	86	100	100	100
Agriculture	88	94	64	86
Urban	88	94	82	100
Barren	80	93	99	93
Forest	79	92	89	95

The most promising feature associated with the object based classification was to establish the difference between 'agriculture' and 'forest' classes. Achieving distinct classification between either of the classes using pixel based classification is quite

Classified

Classified

difficult. Next, fragments of barren land were classified as 'agriculture' in pixel based classification. Such misclassifications were marginally observed in object based method. Further, sandbars were easily identified using object based classification. In the pixel based method sandbars got classified as 'urban' class. However, for comparative analysis, sandbars were included in the 'barren' class. Figure14 presents the classification results for Kshipra basin by object and pixel based methods respectively.

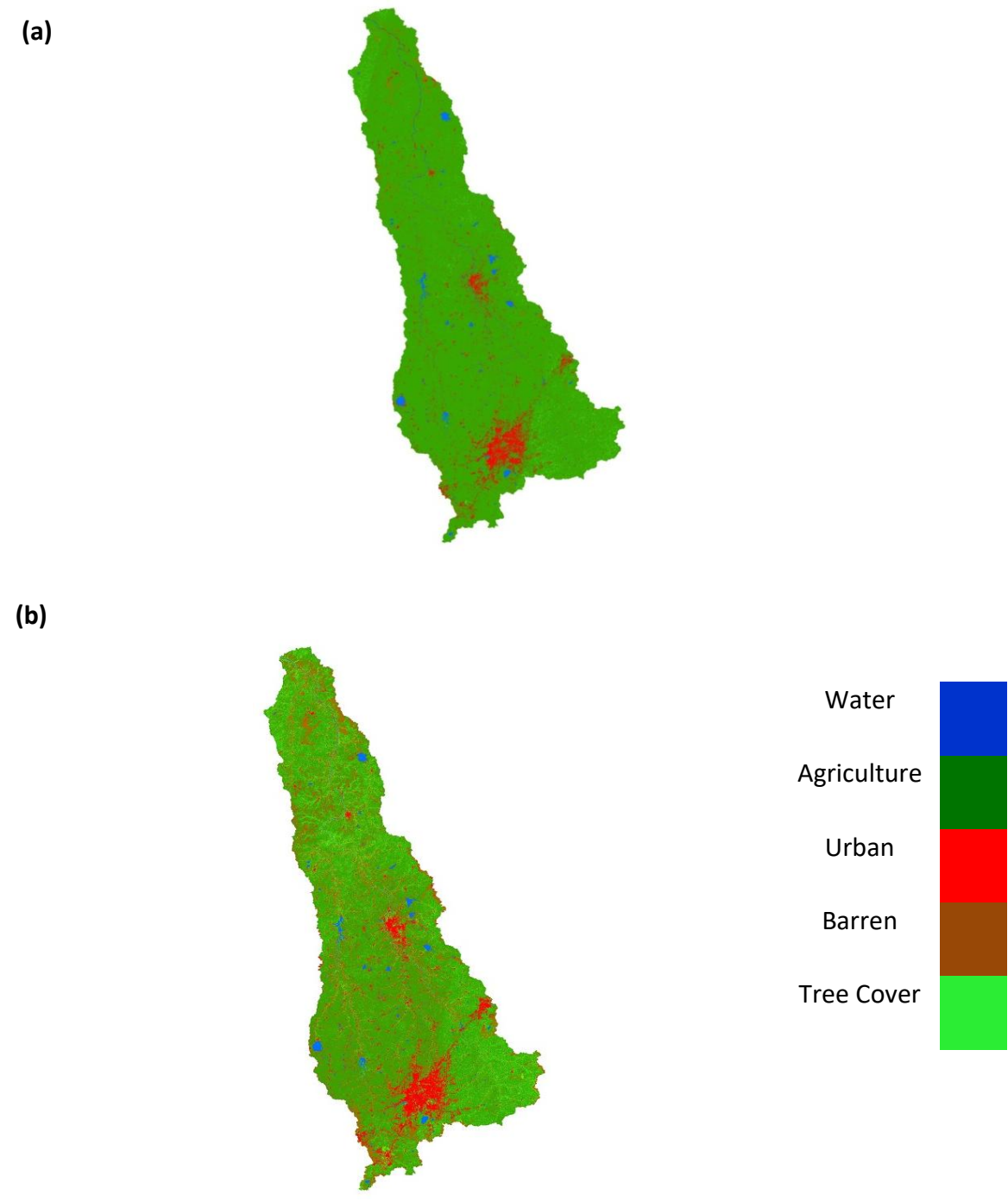


Figure 14: Classification Results from (a) Pixel Based Method and (b) Object Based Method

## 8.2 CORONA Images

#### 8.2.1 Accuracy Assessment of Georeferencing of CORONA Images

As stated in the earlier sections, CORONA image is devoid of spatial information. The geometric distortion involved while scanning the images further increases the complexities of working with this panchromatic historical information. Therefore, georeferencing is inevitable before performing any LULC mapping operation on the CORONA images. However, the accuracy of the assigned spatial information should be assessed in order to obtain the distortions that have occurred during the georeferencing process. In this study, the positional distortions of points, lines and area have been estimated.

Invariant points and landmarks served as the base features for obtaining the accuracy. These points were generally road crossovers. In total, 90 invariant landmarks were selected and their actual co-ordinates were noted using Google Earth (Figure 15). Next, co-ordinates for same points in georeferenced CORONA image are obtained. Their difference is noted and average positional distortion is estimated (Table 7).

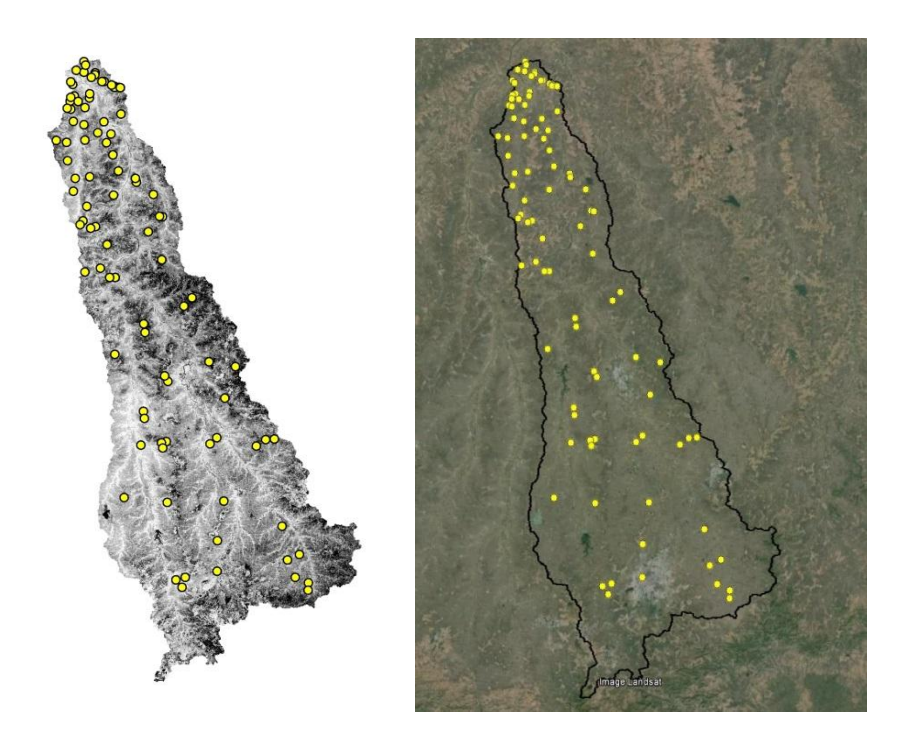


Figure 15: Invariant Points Used for Assessing the Accuracy of Georeferencing

Polygons are generated from the invariant points and their areas were calculated on CORONA and Google Earth respectively. Similarly, lines were formed on joining

random 10 invariant points. The distortions in these lines are reckoned by comparing their lengths on CORONA and Google Earth. Figure 16 (a) and (b) demonstrate a polygon and a line formed from the invariant points.

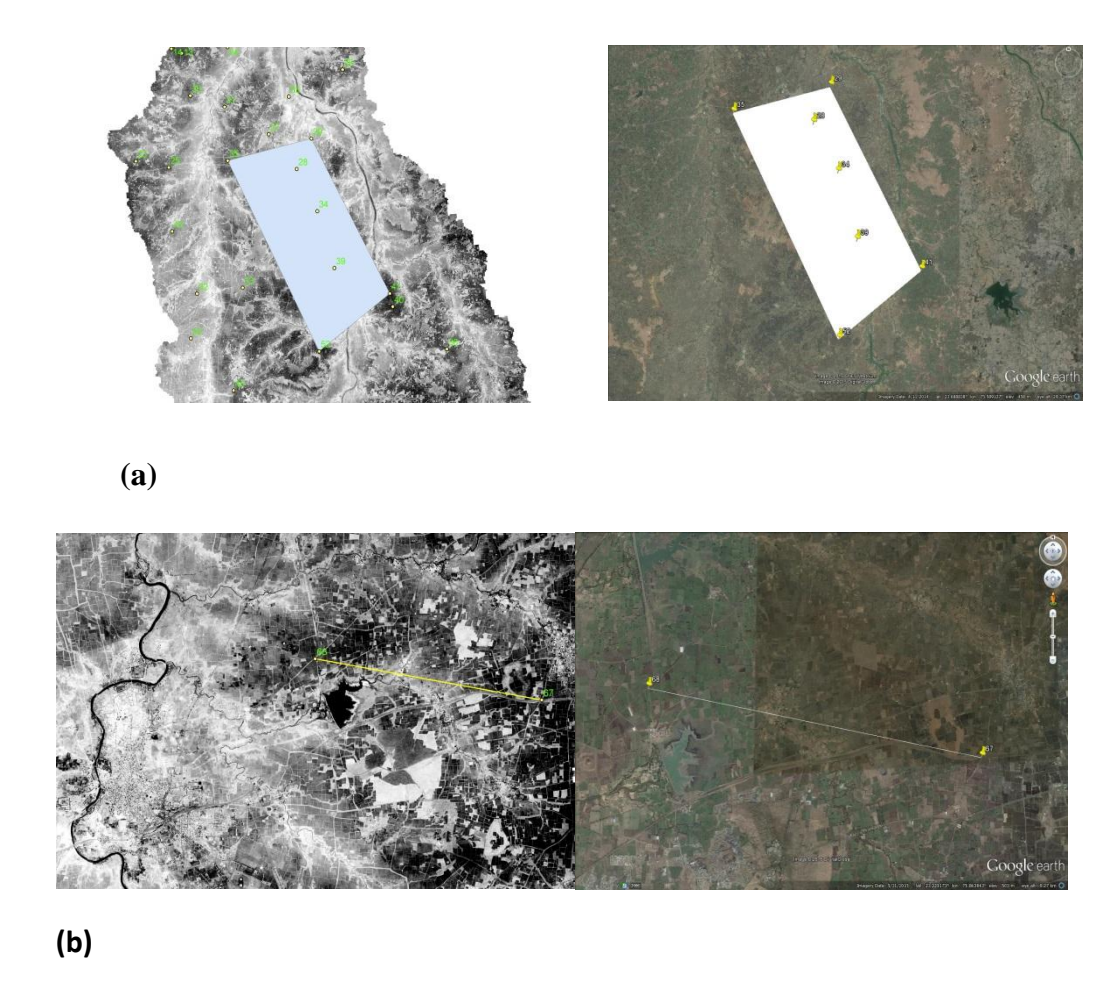


Figure 16: Areas (a) and Lines (b) Formed by the Invariant Points Used for Assessing the Accuracy of Georeferencing

**Table 7: Analysis of Points** 

S. No.	Coi	Corona Google		Earth	Diffe	ence	RMSE (10 <sup>5</sup> m)
	Northing	Easting	Northing	Easting	Northing	Easting	
1	23.884899	75.479897	23.884933	75.47976	3.4E-05	-0.000137	0.000141156
2	23.891001	75.474297	23.89101	75.47425	9E-06	-4.7E-05	4.78539E-05
3	23.9121	75.537697	23.911981	75.537723	-0.000119	2.6E-05	0.000121807
4	23.907801	75.537102	23.907675	75.537002	-0.000126	-0.0001	0.00016086
5	23.938801	75.5093	23.938603	75.509284	-0.000198	-1.6E-05	0.000198645
6	23.914101	75.508797	23.914473	75.508549	0.000372	-0.000248	0.000447088
7	23.930401	75.512703	23.930554	75.512926	0.000153	0.000223	0.00027044
8	23.891399	75.561501	23.891562	75.561452	0.000163	-4.9E-05	0.000170206
9	23.891199	75.555496	23.891202	75.555445	3E-06	-5.1E-05	5.10882E-05
10	23.8577	75.484001	23.857569	75.484084	-0.000131	8.3E-05	0.000155081
11	23.918301	75.488701	23.918231	75.488245	-7E-05	-0.000456	0.000461342
12	23.844801	75.473099	23.844801	75.473099	0	0	0
13	23.8543	75.474998	23.854326	75.474873	2.6E-05	-0.000125	0.000127675
14	23.825701	75.474197	23.825721	75.474095	2E-05	-0.000102	0.000103942
15	23.828699	75.465698	23.828791	75.465576	9.2E-05	-0.000122	0.000152801
16	23.844	75.493698	23.844035	75.49373	3.5E-05	3.2E-05	4.74236E-05
17	23.8522	75.522598	23.852226	75.522448	2.6E-05	-0.00015	0.000152237
18	23.880199	75.587601	23.880008	75.58781	-0.000191	0.000209	0.000283129
19	23.8776	75.5877	23.877864	75.587611	0.000264	-8.9E-05	0.000278598
20	23.8829	75.580399	23.882887	75.580366	-1.3E-05	-3.3E-05	3.54683E-05
21	23.8766	75.602402	23.876396	75.602288	-0.000204	-0.000114	0.000233692
22	23.862499	75.524002	23.862671	75.524112	0.000172	0.00011	0.000204167
23	23.9018	75.527901	23.901752	75.527866	-4.8E-05	-3.5E-05	5.94054E-05
24	23.7519	75.436798	23.7519	75.436798	0	0	0
25	23.8298	75.510902	23.8298	75.510902	0	0	0
26	23.747601	75.463402	23.74763	75.463409	2.9E-05	7E-06	2.98329E-05
27	23.813999	75.603699	23.813901	75.603545	-9.8E-05	-0.000154	0.000182538
28	23.7701	75.543999	23.770159	75.543917	5.9E-05	-8.2E-05	0.00010102
29	23.746201	75.566399	23.746265	75.566343	6.4E-05	-5.6E-05	8.50412E-05

30	23.767	75.5783	23.767132	75.57819	0.000132	-0.00011	0.000171825
31	23.7967	75.480904	23.796566	75.480966	-0.000134	6.2E-05	0.000147648
32	23.7889	75.508499	23.78918	75.508734	0.00028	0.000235	0.000365548
33	23.661301	75.485802	23.66128	75.486261	-2.1E-05	0.000459	0.00045948
34	23.6653	75.522598	23.665262	75.522622	-3.8E-05	2.4E-05	4.49444E-05
35	23.7174	75.582802	23.717211	75.582918	-0.000189	0.000116	0.000221759
36	23.7521	75.510803	23.752157	75.510821	5.7E-05	1.8E-05	5.97746E-05
37	23.5695	75.710297	23.569076	75.710073	-0.000424	-0.000224	0.000479533
38	23.570601	75.702301	23.570383	75.702154	-0.000218	-0.000147	0.000262932
39	23.6227	75.686798	23.622859	75.686667	0.000159	-0.000131	0.000206015
40	23.6784	75.596497	23.678306	75.596645	-9.4E-05	0.000148	0.000175328
41	23.651899	75.643303	23.651872	75.643501	-2.7E-05	0.000198	0.000199832
42	23.660801	75.640999	23.660994	75.641009	0.000193	1E-05	0.000193259
43	23.6308	75.480797	23.630808	75.480694	8E-06	-0.000103	0.00010331
44	23.703899	75.465897	23.703453	75.465969	-0.000446	7.2E-05	0.000451774
45	23.560801	75.505096	23.560998	75.504874	0.000197	-0.000222	0.000296805
46	23.5951	75.5149	23.594971	75.514818	-0.000129	-8.2E-05	0.000152856
47	23.5466	75.5373	23.5466	75.5373	0	0	0
48	23.5427	75.525101	23.542615	75.524994	-8.5E-05	-0.000107	0.000136653
49	23.5518	75.497704	23.551996	75.497415	0.000196	-0.000289	0.000349195
50	23.3566	75.764099	23.35635	75.764218	-0.00025	0.000119	0.000276877
51	23.3764	75.785301	23.376601	75.785401	0.000201	1E-04	0.000224502
52	23.5336	75.672997	23.53369	75.673001	9E-05	4E-06	9.00888E-05
53	23.621599	75.584	23.621541	75.583907	-5.8E-05	-9.3E-05	0.000109604
54	23.7957	75.560303	23.795613	75.559911	-8.7E-05	-0.000392	0.000401538
55	23.4256	75.587303	23.425592	75.587334	-8E-06	3.1E-05	3.20156E-05
56	23.425501	75.573502	23.425507	75.573434	6E-06	-6.8E-05	6.82642E-05
57	23.447901	75.5495	23.447878	75.549439	-2.3E-05	-6.1E-05	6.5192E-05
58	23.4389	75.509697	23.438938	75.509516	3.8E-05	-0.000181	0.000184946
59	23.503599	75.5672	23.503592	75.567193	-7E-06	-7E-06	9.89949E-06
60	22.688299	75.755402	22.688445	75.755416	0.000146	1.4E-05	0.00014667
61	22.712099	75.764	22.7121	75.764088	1E-06	8.8E-05	8.80057E-05
62	22.7061	75.740402	22.706105	75.740331	5E-06	-7.1E-05	7.11758E-05

					Avera	age Error	0.0001703
90	22.7108	76.046097	22.710748	76.045886	-5.2E-05	-0.000211	0.000217313
89	22.6971	76.079597	22.696992	76.079358	-0.000108	-0.000239	0.000262269
88	23.039801	75.994904	23.039639	75.994969	-0.000162	6.5E-05	0.000174554
87	23.0235	75.9487	23.0235	75.9487	0	0	0
86	23.0382	75.972801	23.03848	75.972773	0.00028	-2.8E-05	0.000281397
85	23.02	75.707901	23.020191	75.708018	0.000191	0.000117	0.000223987
84	23.032499	75.704498	23.032404	75.70455	-9.5E-05	5.2E-05	0.000108301
83	23.035299	75.7173	23.035329	75.717271	3E-05	-2.9E-05	4.17253E-05
82	22.9027	75.607903	22.902843	75.60792	0.000143	1.7E-05	0.000144007
81	23.027201	75.6521	23.027201	75.6521	0	0	0
80	22.7992	75.847397	22.799657	75.8473	0.000457	-9.7E-05	0.000467181
79	22.726101	75.846001	22.725908	75.846013	-0.000193	1.2E-05	0.000193373
78	22.890699	75.7192	22.890969	75.71919	0.00027	-1E-05	0.000270185
77	23.2428	75.585701	23.242732	75.585879	-6.8E-05	0.000178	0.000190547
76	23.090099	75.661003	23.090117	75.661097	1.8E-05	9.4E-05	9.57079E-05
75	23.107599	75.658897	23.107466	75.658785	-0.000133	-0.000112	0.000173876
74	23.4676	75.708199	23.467483	75.70813	-0.000117	-6.9E-05	0.000135831
73	23.294901	75.663696	23.294808	75.663848	-9.3E-05	0.000152	0.000178194
72	23.315001	75.660202	23.314844	75.660324	-0.000157	0.000122	0.000198829
71	23.191	75.713997	23.190965	75.714127	-3.5E-05	0.00013	0.000134629
70	23.177999	75.721703	23.178	75.7217	1E-06	-3E-06	3.16228E-06
69	23.2241	75.828499	23.224229	75.828692	0.000129	0.000193	0.000232142
68	23.2124	75.895798	23.2122	75.895968	-0.0002	0.00017	0.000262488
67	23.1374	75.868202	23.137404	75.868351	4E-06	0.000149	0.000149054
66	22.892799	75.864304	22.892905	75.864228	0.000106	-7.6E-05	0.00013043
65	22.8326	76.013199	22.83253	76.012974	-7E-05	-0.000225	0.000235637
64	22.7521	76.026802	22.752036	76.026757	-6.4E-05	-4.5E-05	7.82368E-05
63	22.764999	76.056999	22.764807	76.05697	-0.000192	-2.9E-05	0.000194178

An average positional error of approximately 17 meters is acceptable. It reflects that any point on the CORONA image will lie inside the radius of 17 meters of its actual position as the center. Due to the fact that CORONA data suffers from an inbuilt distortion, deviation between the actual position and position on the image for these points is observed.

Similarly, the error percentage between the lengths and areas for the generated lines and polygons are calculated. Average percentage error of 0.126 is obtained as shown in Table 8. This means that there is an error of 1.26 m per kilometer in the image. In Table 9 average percentage error of 0.143 indicates that for every square kilometer, average error in area is 1430 square meters. Beside these values can be attributed to the geometric distortion. They are acceptable as these errors will not affect much on the final results.

**Table 8: Analysis of Lines** 

**Table 9: Analysis of Areas** 

S. No.	Length of line from Google Earth	Length of line from CORONA Image	Difference	Error %
1	7.01	6.9823	0.0277	0.395
2	3.1	3.08978	0.01022	0.330
3	11	11.0259	-0.0259	-0.235
4	11.2	11.2107	-0.0107	-0.096
5	38.21	38.1192	0.0908	0.238
			Average Error	0.126

S. No.	Area of Polygon from Google Earth	Area of Polygon from CORONA Image	Difference	Error %
1	5.66132	5.67285	0.01153	0.204
2	10.957	10.97136	0.01436	0.131
3	103.958	103.99	0.032	0.031
4	281.082	281.56	0.478	0.170
5	538.461	539.433	0.972	0.181
			Average Error	0.143

### 8.2.2 CORONA Image Classification

Not much of the study has been done to classify the CORONA data using object based classification technique. Manual classification of these images is done in past. However, classifying each pixel to its desired class is time consuming and laborious.

The classification of CORONA image was performed using object based technique. The LULC map was obtained by combining pixel information with the contextual and textural information available on segmenting the image. Figure 17 shows classified map of KRB in the year 1965.

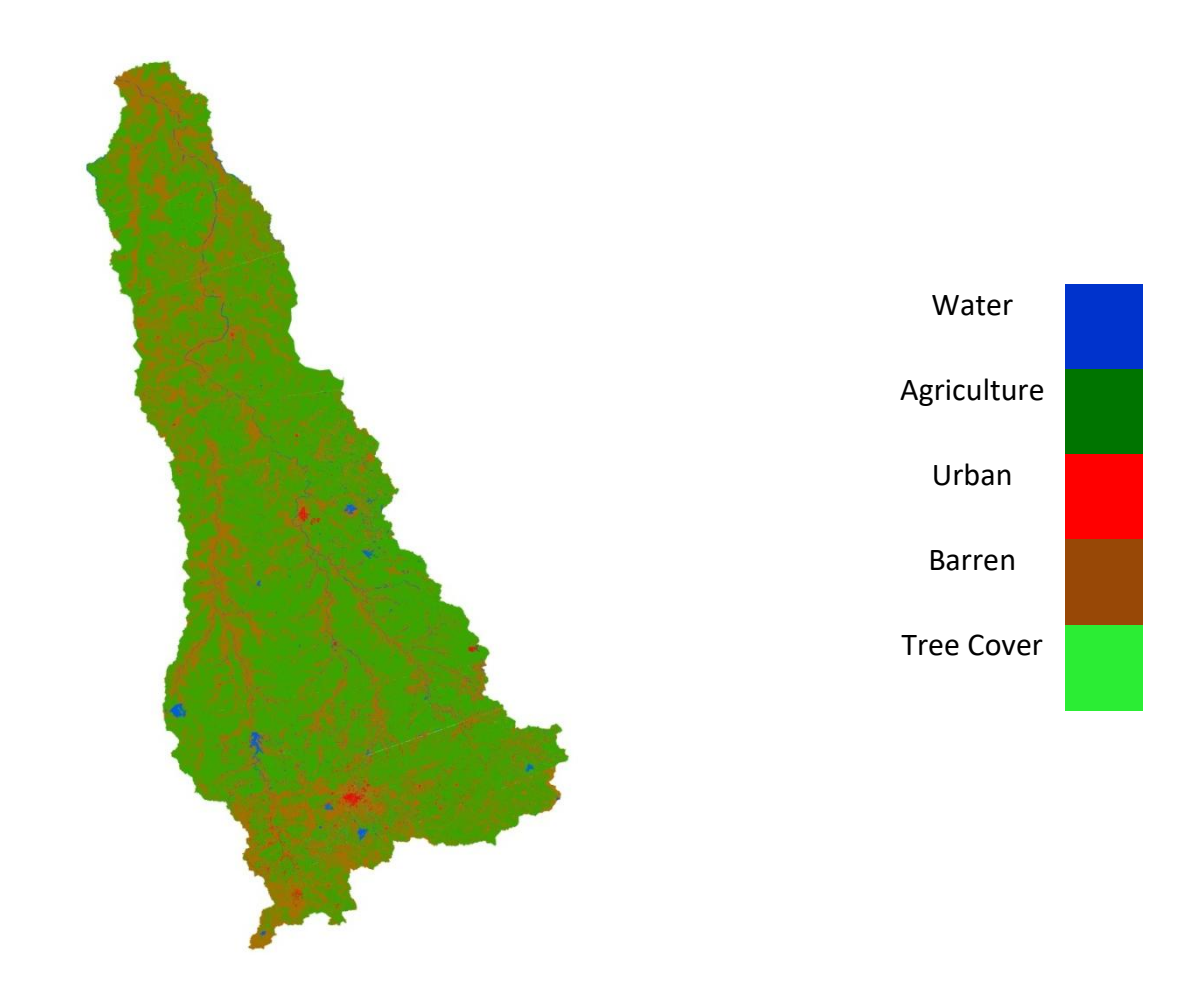


Figure 17: Classification Results of CORONA Image

The accuracy assessment for the classified map was done by carefully selecting the landmarks that have not been altered. For every class, 50 invariant points lying inside an unchanged land cover area were selected and then matched with their corresponding classes in classified image. Figure 18 shows the position of these random points on the raw and classified CORONA images.

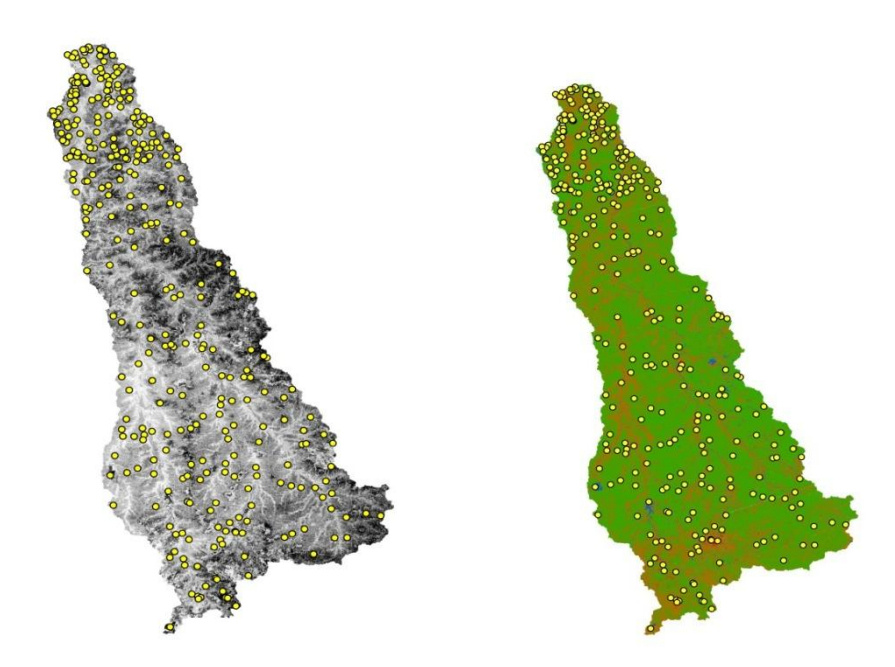


Figure 18: Invariant Points Selected for Accuracy Assessment of Classified CORONA Image

An error matrix is developed on the basis of these invariant points as shown in Table 10. The overall accuracy of 86.8% is obtained. Misclassification was observed between water and agriculture class. This can be attributed to the similar pixel values. Similarly, forest areas have also been misclassified with water. The misclassifications among the classes can be checked by manually rectifying them. The user's and producer's accuracy are preseted in Table 11.

Table 10: Error Matrix for CORONA Image Classification Referenced

Classes	Water	Agriculture	Urban	Barren	Forest	Total
Water	41	5	0	0	4	50
Agriculture	0	47	0	3	0	50
Urban	0	4	42	2	2	50
Barren	0	3	1	46	0	50
Forest	7	2	0	0	41	50
Total	48	61	43	51	47	250

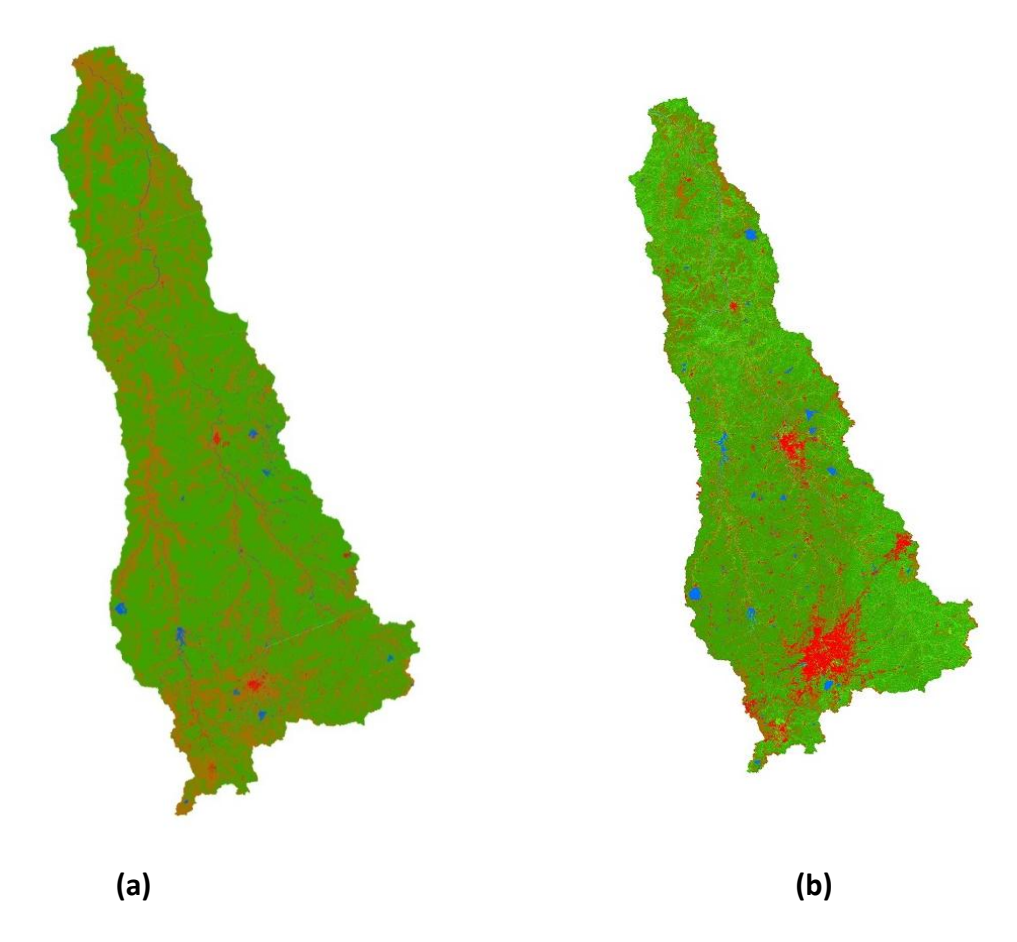
Table 11: User's and Producer's Accuracy for CORONA Image Classification

Classes	User Accuracy (%)	Producer Accuracy (%)	
Water	82	85	
Agriculture	94	77	
Urban	84	97	
Barren	92	90	
Forest	82	87	

Classified

## 8.2.3 LULC Change Detection

The classification results from object based method for LISS IV and CORONA images can be compared to obtain the LULC change between years 1965 and 2013 respectively (Figure 19 (a) and (b)).



The percentage of land covers of each class is shown in Table 12.

Table 12: Percentage Area in KRB from CORONA and LISS IV Images

Classes	Percentage Area	
	CORONA (1965)	LISS IV (2013)
Agriculture	62.59	62.87
Urban	0.9	7.79
Water	1.6	1.55
Tree Cover	0.78	11.97
Barren	34.13	15.82

The percentage area of water class is almost similar. However, on close inspection of the classified images, it can be observed that the number of reservoirs has increased in comparison to the year 1965. Though Kshipra and its tributaries are seasonal, yet water is available in the river for most part of the year. This water majorly comes from

Narmada River Valley Project in which Kshipra is fed with substantial quantities of water. And, the presence of check dams and barrages has ensured the storage of water.

Though the relative percentage of water area is not significantly different in both images, ground inspection has revealed that the water quality in Kshipra and its tributaries is of much deteriorated quality. This signifies that the water carried by river is mostly sewage coming out of the major towns like Indore, Dewas and Ujjain. Hence, good water is not available in the river. Field surveys in and around the city of Indore shows that Kanh River carries sewage of Indore city throughout the year and dumps it in river Kshipra near Ujjain.

The percentage of agricultural land has remained almost same in year 2013 as compared to 1965. The sewage water flowing in river is used up by farmers to irrigate the fields. This has ensured that the agricultural land is not converted into barren lands in the absence of natural water during non-monsoon period.

Urban area has increased from 0.9% to 7.79% since 1965. This change has majorly occurred due to rapid urbanization that has occurred in the KRB. Road connectivity between the towns and conversion of unpaved roads into paved roads has increased and contributes to the urban cover.

Urban sprawl is also observed in the towns of Indore, Ujjain and Dewas. Ground surveys have indicated that encroachment at the banks has reduced the width of the river. Buildings and houses near banks pollute the river directly and create unhygienic environment in the vicinity of river.

Tree cover and plantation area has considerably increased since 1965. The growing awareness among people and stringent government rules for cutting trees and promotion of afforestation can be attributed for this positive change. A lot of plantation is observed along the road sides. The barren lands of 1965 also possess a good tree cover in 2013 near the major cities.

Barren area has reduced to nearly 15% from 34% in 1965. The rapid urbanization and increase in developmental activities have resulted in conversion of barren into urban areas. But, there should be a limit to the urban expansion into barren areas. If uncontrolled urban growth continues then it may result in non-judicious use of the available natural resources.

# 9. Summary and Conclusions

With the finer resolution satellite imageries, detecting accurate land features has become inevitable for any classification method. Results from this study show that land cover mapping can be obtained with an enhanced accuracy by using object based method instead of pixel based method. This is attributed to the ability of object based method to incorporate spatial information in conjunction with the spectral information of the images. Classification accuracy of 94.6% is obtained by object based method in comparison to the 84.2% by pixel based method.

Besides better overall accuracy, object based classification method was able to distinctly classify sandbars which were classified into 'urban' class in pixel based method. A lot of misclassification was observed between agriculture and forest areas while analyzing the pixel based classification results. Object based classification was able to remove the shortcomings in pixel based methods and produced an accurate classified map for the images.

The pan-chromatic CORONA data is a very important source of historical information. However, producing a land cover map using these images is not easy. Object based classification was carried out on CORONA images with an overall accuracy of 86.8%. In order to enhance the accuracy, manual rectification of wrongly classified objects is required. Classifying the meaningful objects rather than individual pixels reduces the efforts required for obtaining a reasonable mapping.

LULC changes have been observed by comparing the classified LISS IV and CORONA images of the years 2013 and 1965 respectively. Results show that barren land has reduced from 34.2% to 15.4%. This is attributed to the increment in the tree cover and urban areas. The percentage of water and agricultural areas has not differed significantly in KRB. However, state-of-the-art as of now does not permit any assessment of water quality using satellite imagery. The river should flow with the fresh water and not just be the medium to carry sewage of the towns in KRB.

# 10. Future Scope

Object based techniques have been seldom applied on the pan-chromatic datasets. This study shows that these kinds of historical images can be classified with reduced human efforts and acceptable accuracy. However, in order to enhance the accuracy some manual corrections are needed to be done. These images are of very fine resolution meaning that more number of classes can be extracted out. For this, after

applying the regular set of algorithms, some manual delineation of the classes of interest on the image datasets will be required.

Another aspect that can be carried forward with the LULC information is to study the hydrology and ecology of any basin. A detailed land cover data can be incorporated into the software's like SWAT and hydrological responses can be recorded.

One of the major challenges that one faces while working with CORONA images is its georeferencing and automated processing. It will reduce a lot of efforts if these historical images can be handled by an automated process. So, developing software which could reduce the manual efforts in processing of these images can be an interesting work.

# References

Asian Development Bank Report (2011). Support to the National Water Mission, NAPCC. Appendix 3 Kshipra Sub-basin.

Andersen, G.L.(2006). How to detect desert trees using CORONA images: discovering historical ecological data. *Journal of Arid Environments*, 65. pp. 491–511.

Aplin, P., Atkinson, P. and Curran, P. (1999). Per-field classification of land use using the forthcoming very fine resolution satellite sensors: problems and potential solutions. *Advances in Remote Sensing and GIS Analysis*. Wiley and Son, Chichester. pp. 219–239.

Baatz, M. and Schipe, A. (1999). Object-oriented and multi-scale image analysis in semantic networks. *In*: Proc. of the 2nd International Symposium on Operationalization of Remote Sensing.

Baatz, M., Benz, U. and Dehghani, S. (2004). eCognition User Guide 4, Definiens Imagine. http://www.Definiens-imaging.com.

Benz, U. C., Hofmann, P., Willhauck, G., Lingenfelder, I. and Heynen, M. (2004). Multiresolution, object-oriented fuzzy analysis of remote sensing data for GIS-ready information. *ISPRS Journal of Photogrammetry & Remote Sensing*. pp.239–258.

Bitelli, G., and V.A. Girelli (2009). Metrical use of declassified satellite imagery for an area of archaeological interest in Turkey. *Journal of Cultural Heritage*, 10 (Supplement 1).pp. 35–40.

Blaschke, T. and Hay, G. (2001). Object-oriented image analysis and scale-space: theory and methods for modeling and evaluating multi-scale landscape structures. *International Archives of Photogrammetry & Remote Sensing*, 34(4/W5). pp.22–29.

Blaschke, T. and Strobl, J. (2001). What's wrong with Pixels? Some recent developments interfacing remote sensing and GIS. Geo- BIT/GIS, 6: 12–17.

Blaschke, T., Lang, S. and Hay, G. (2008). Object-Based Image Analysis, Spatial Concepts for Knowledge-Driven Remote Sensing Applications, Series: *Lecture Notes in Geoinformation and Cartography, Springer*.

Carleer, A.P. and Wolff, E. (2006).Region-based classification potential for land-cover classification with very high spatial resolution satellite data.*In*: Proceedings of 1st International Conference on Object-based Image Analysis, Salzburg University, Austria, July 4-5, 2006. Vol. XXXVI.

Casana, J., Cothren, J. (2008). Stereo analysis, DEM extraction and ortho-rectification of CORONA satellite imagery: archaeological applications from the Near East. *Antiquity* 82. pp. 732–749.

Dashora, A., Lohani, B. and Malik, J.N. (2007). A repository of earth resource information – CORONA satellite programme. *Current Science*, *92(7)*. pp. 926–932.

Dey, V., Zhang, Y. and Zhong, M. (2010). A review on image segmentation techniques with remote sensing perspective. *IAPRS*, *Vol. XXXVIII*, *Part 7A*.

Fowler, M.J.F. (2004). Declassified CORONA KH-4B satellite photography of remains from Rome's desert frontier. *International Journal of Remote Sensing*, 25(18). pp. 3549–3554.

Fowler, M.J.F. (2005).An evaluation of scanned CORONA intelligence satellite photography, *AARGnews*, *31*. pp. 34–37.

Franklin, J., Woodcock, C. E., and Warbington, R. (2000). Multi-Attribute Vegetation Maps of Forest Services Lands in California Supporting Resource Management Decisions. *Photogrammetric Engineering & Remote Sensing*.

Galiatsatos, N. (2004). Assessment of the CORONA Series of Satellite Imagery for Landscape Archaeology. A Case Study from the Orontes Valley, Syria, Ph.D. dissertation, University of Durham, Durham.

Galiatsatos, N. (2009). The shift from film to digital product: focus on CORONA imagery. *Photogram. – Fernerkundung – Geoinform*. pp. 251–260.

Gheyle, W. (2009). Highlands and Steppes. An Analysis of the Changing Archaeological Landscape of the Altay Mountains from the Eneolithic to the Ethnographic Period, Ph.D. dissertation, Ghent University, Ghent.

Gheyle, W., Trommelmans, R., Bourgeois, J., Goossens, R., Bourgeois, I., De Wulf, A. and Willems, T. (2004). Evaluating CORONA: A case study in the Altai Republic (South Siberia). *Antiquity*, *78*(300). pp. 391–403.

Haralick, R. and Shapiro, L. (1992). Computer and Robot Vision, vol. I. Chap. 9. Texture. Addison-Wesley, Reading, USA.pp. 453–494.

Hay, G. and Blaschke, T. et al. (2003). A comparison of three image-object methods for the multiscale analysis of landscape structure. *Journal of Photogrammetry and Remote Sensing*, 57. pp. 327–345.

Hay, G. and Castilla, G. (2006). Object-based image analysis: Strengths, weaknesses, opportunities and threats. *In*: 1st International Conference on Object-based Image Analysis, Salzburg.

Kennedy, D. (1998). Declassified satellite photographs and archaeology in the Middle East: Case studies from Turkey. *Antiquity*, 72(277). pp. 553–61.

Leachtenauer J., Daniel, K. and Vogl, T. (1994). Digitizing Satellite Imagery: Quality and Cost Consideration, *Photogrammetric Engineering and Remote Sensing*, vol 64.p.p. 29-34.

Lillesand, T. and Kiefer, R. (2000). Remote Sensing and Image Interpretatio, New York, USA: John Wiley & Sons.

Mather, P. (1999). Computer processing of remotely-sensed images, Chichester: Wiley.

McDonald R.A. (1995). Corona: Success for Space Reconnaissance, A Look into the Cold War, and a Revolution for Intelligence. *Photogrammetric Engineering & Remote Sensing*, vol 61. p.p. 689-720.

NRO Report (1967). CORONA J-3 System Handbook, Record 3/C/0014 of the collection of CORONA, ARGON and LANYARD records.

Pacifici, F., Chini, M. and Emery, W.J. (2009). A neural network approach using multiscale textural metrics from very high-resolution panchromatic imagery for urban landuse classification. *Remote Sens. Environ.*, 113, 1276–1292.

Pal, N. R. and Pal, S. K. (1993). A review on image Segmentation techniques. *Pattern Recognition*, 26(9), pp. 1274-1294.

Pesaresi, M. (1999). Textural classification of very high-resolution satellite imagery: empirical estimation of the interaction between window size and detection accuracy in urban environment. *In*: Proc. ICIP, vol. 1. pp. 114–118.

Richards, J.A. (1993). Remote Sensing Digital Image Analysis: An Introduction, 2nd ed Springer-Verlag, Berlin.

Roerdink, M. and Meijster, A. (2001). The watershed transform: definitions, algorithms and parallelization strategies. *Fundament.Informat.*, *41*. pp. 187–228.

Sarkar, D. (2014). Assessment of human disturbances on the Ganga river system around Kanpur.

Sateesh, K. and Sandip, G. (2011).Land use and Land cover mapping using digital classification technique in Tikamgarh district, Madhya Pradesh, India using Remote Sensing.*International Journal of Geomatics and Geosciences*, *2*(*2*). pp. 519-529.

Schiewe, J. (2002). Segmentation of high-resolution remotely sensed data concepts, applications and problems. *Symposium on Geospatial Theory, Processing and Applications*.

Shaban, M.A., Dikshit, O. (2001). Improvement of classification in urban areas by the use of textural features: the case study of Lucknow city, Uttar Pradesh. *Int. J.Rem. Sens. 22*. pp. 565–593.

Shackelford A. K., and Davis C. H. (2003). A combined fuzzy pixel-based and object-based approach for classification of high-resolution multispectral data over urban areas. *IEEE Transactions on Geoscience and Remote Sensing*, 41. pp. 2354-2364.

Sharma, N., Mishra, M. and Shrivastava, M. (2012). Colour image segmentation techniques and issues: an approach, *International Journal of Scientific & Technology ResearchVolume 1*.

Shi, J. and Malik, J. (1997). Normalized Cuts and Image Segmentation. *IEEE Conference on Computer Vision and Pattern Recognition*. pp. 731-737.

Singh, K. and Singh, A. (2010). A Study of Image Segmentation Algorithms for Different Types of Image. *International Journal of Computer Science Issues*, Vol. 7.

Stumpf, A. and Kerle, N. (2011). Object-oriented mapping of landslides using Random Forests. *Remote Sensing of Environment*, 115. pp. 2564-2577.

Tappan G.G., Hadj, A., Wood, C.E. and Lietzow, R.W. (2000). Use of Aragon, Corona, and Landsat Imagery to Assess 30 Years of Land Resource Changes in West-Central Senegal. *Photogrammetric Engineering & Remote Sensing*, vol 66.p.p. 727-735.

Tian, J. and Chen, D.M. (2007). Optimization in multi-scale segmentation of high-resolution satellite images for artificial feature recognition. *International Journal of Remote Sensing*, *28*(20). pp. 4625-4644.

Tso, B. and Mather, M. (2001). Classification Methods for Remotely Sensed Data. Taylor and Francis, London.

UR, J. (2003). CORONA satellite photography and ancient road networks: a Northern Mesopotamian case study. *Antiquity*, 77. pp. 102–115.

Varshney, S.S., Rajpal, N. and Purwa, R. (2009). Comparative Study of Image Segmentation Techniques and Object Matching using Segmentation. *In:* Proceeding of International Conference on Methods and Models in Computer Science. pp. 1-6.

Wardell A.D., Reenberg, A. and Tottrup, C. (2003). Historical footprints in contemporary land use systems: forest cover changes in savannah woodlands in the Sudano-Sahelian zone. *Global Environmental Change, vol 13*. p.p. 235-254.

Zhang, Y. J. (1997). Evaluation and comparison of Different segmentation algorithms. *Pattern Recognition Letters*, 18(10). pp. 963-974.